Environmental Nanotechnology, Monitoring & Management 14 (2020) 100295

Contents lists available at ScienceDirect

Environmental Nanotechnology, Monitoring & Management

journal homepage: www.elsevier.com/locate/enmm

Chitosan stabilized Fe/Ni bimetallic nanoparticles for the removal of cationic and anionic triphenylmethane dyes from water

Anju Rose Puthukkara P., Sunil Jose T.*, Dinoop lal S.

Dept. of Chemistry, St. Thomas' College, Thrissur, Kerala 680 001, India

ARTICLE INFO

Keywords:
Zero valent iron
Chitosan
Fe/Ni bimetallic nanoparticles
Triphenylmethane dye

ABSTRACT

A comparative investigation has been carried out for the effective removal of cationic and anionic triphenylmethane dyes from the water using zero valent iron and iron/nickel bimetallic nanoparticles stabilized by chitosan (CS). The biopolymer chitosan, used as a stabilizer in this study is biodegradable and non-toxic. Chitosan stabilized zero valent iron (CS-Fe) and Chitosan stabilized bimetallic iron/nickel (CS-Fe/Ni) nanoparticles were prepared by chemical reduction method using sodium borohydride as reducing agent under nitrogen atmosphere. The characteristics of CS-Fe/Ni, CS-Fe and CS nanoparticles were examined by HRTEM, XPS, Zeta Potential, zeta potential and FTIR. HRTEM results reveal that iron nanoparticles were successfully coated with chitosan and the prepared particles were in nano dimensions. The average size of these synthesized nanoparticles was below 15 nm. The interaction of hydroxyl and amino groups of chitosan with iron in CS-Fe/Ni and CS-Fe nanoparticles was confirmed by FTIR. The surface compositions of the nanoparticles obtained from the XPS analysis revealed the presence of zerovalent iron and nickel in chitosan. Batch experiments were carried out to evaluate the removal efficiencies of CS-Fe/Ni, CS-Fe and CS in the triphenylmethane dyes. The model pollutants selected for dye removal study were cationic malachite green dye and anionic methyl blue dye. The parameters studied in the dye removal were effects of dosage of the nanoparticle, contact time, initial concentration of the dyes, solution pH and ionic strength. The results indicate that CS-Fe/Ni nanoparticles are more effective in dye removal compared to CS-Fe nanoparticles and CS.

1. Introduction

Water pollution has turned out to be one of the major environmental problem faced by the world which is drastically influenced by the population stress and industrialization. Every year thousands of people are dying or diseased by consuming the polluted water. The waste dyes from textiles, paper, rubber, plastics, leather, cosmetics, pharmaceuticals and food industries have become one of the major culprits of the widespread water pollution. Dyes not only reduces the light penetration and photosynthesis in water bodies but also acts a toxic, mutagenic and carcinogenic agent in living cells. The conventional techniques (coagulation and flocculation, oxidation, ozonation and activated carbon adsorption) have not shown considerable efficiency and economic advantage. Biodegradation of dye molecules is much difficult due to its complex aromatic molecular structure. Removal of dyes has been studied through different technologies and by using numerous inorganic and biological adsorbents (Batool et al., 2014; Raman and Kanmani, 2016). Over the last few decades, implementation of nanotechnology to replace conventional water contamination remediation techniques were being practised using the unique properties of nanomaterials. Application of different nanomaterials like carbon nanotubes, nano filters, nanoscale zero valent metals, nanomembranes etc., would be a platform to a wide variety of opportunities for the purification of polluted water and to provide low-cost clean water (Amin et al., 2014; Tesh and Scott, 2014). Among these materials, nanoscale iron and iron oxide particles have a remarkable position due to its low cost, environmental compatibility and high reactivity (Li et al., 2006).

The nanoscale elemental iron (nFe°) is considered as a potential green material to remediate wastewater due to the availability of iron as recycled material and its capacity to degrade some contaminants completely. The application of zero valent iron for the treatment of wastewater which contains organic contaminants, toxic metals and inorganic compounds have been studied and a supreme activity for pollutant removal was established through previous studies (Fu et al., 2014; Yan et al., 2013). Reduction, sorption, complexation, and co-precipitation are the main pathways of mechanism for the degradation of these pollutants. Magnetic properties and non-toxicity are also the advantages of the nFe° particles. Even though nFe° show high reactivity

* Corresponding author.
E-mail address: sjtppc@gmail.com (S.J. T.).

https://doi.org/10.1016/j.enmm.2020.100295
Received 24 December 2019; Received in revised form 9 March 2020; Accepted 10 April 2020

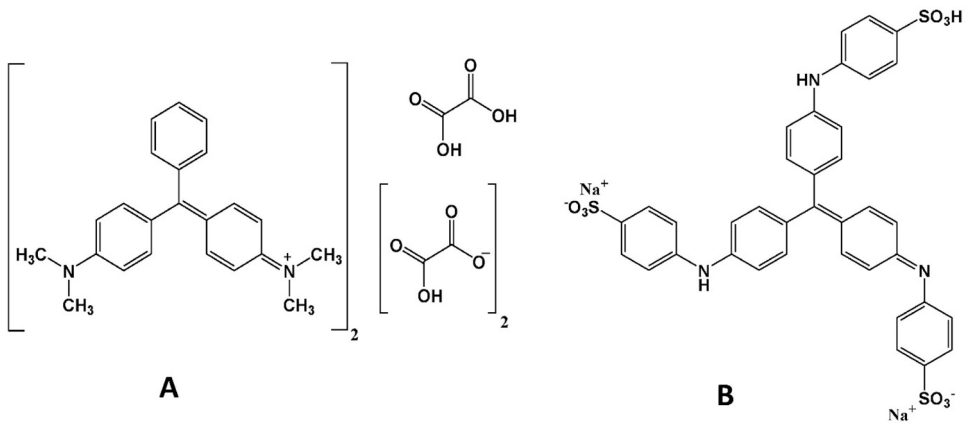

Fig. 1. Chemical structure of Malachite Green (A) and Methyl Blue (B) (For interpretation of the references to colour in this figure legend, the reader is referred to the web version of this article).

towards pollutants, the major limitations of them are reactivity loss with time due to the precipitation of iron oxides on the surface of Fe° and their agglomeration tendency due to magnetic properties (Raychoudhury and Scheytt, 2013; Yirsaw et al., 2016). The catalytic properties of monometallic Fe° can be improved to a large magnitude through bimetallization. The addition of a second metal to the Fe° enhances the properties of iron through the synergetic effect of two distinct metal which serves as a protective agent against corrosion of the iron surface. Till now different iron-based bimetallic nanoparticles such as Fe/Al, Fe/Pd, Fe/Ni, Fe/Cu, Fe/Zn, Fe/Ag, Fe/Au, Fe/Co and Fe/Pt were synthesized and its catalytic elimination properties were studied in various pollutants (Liu et al., 2014; Sharma et al., 2017). Cost-effectiveness and toxic effect of second metal could also be considered as two important criteria for the selection of second metal on water pollution remediation. Among the synthesised bimetallic nanoparticles, Fe/Ni nanoparticles have special focus because of its ability to enhance the formation of atomic hydrogen on the surface of Fe° which hinders the iron oxide formation on the surface of Fe°. This would yield more hydrogen radicals produced from H_2 decomposition. In addition to this, catalytic metal Ni is less toxic and economically feasible compared to other catalytic metals (Ezzatahmadi et al., 2019; Foster et al., 2019; Gao et al., 2016; Weng et al., 2014).

Although Fe° and Fe/Ni nanoparticles get considerable attention due to their high specific surface area and small size, the nFe° particles are highly reactive towards air and water. To develop the Fe° and Fe/Ni nanoparticles as an efficient remediating agent, they could be modified or combined with different methods. Mostly these methods are Immobilization of nFe° onto supports like zeolite, polymers, etc and combine nFe° with other techniques like sonication and UV irradiation (Adusei-Gyamfi and Acha, 2016). Even though the stabilization of Fe° is extensively studied, further investigation is needed for the stabilization of Fe° and Fe/Ni nanoparticles due to its potential capacity for water contaminant degradation and small footprint. In this study, we are incorporating chitosan, a biopolymer, with Fe° and Fe/Ni nanoparticles. Only limited studies have presently been reported on stabilization of Fe° nanoparticles by chitosan. Chitosan is a biopolymer produced by deacetylation of chitin, which is derived from the exoskeleton of crustaceans and cartilages of molluscs. The presence of free amino and hydroxyl groups in chitosan makes them material with high adsorption potential and multipurpose materials in industrial applications. The other favourable characteristics of chitosan as an adsorbent are its macromolecular structure, non-toxicity, biocompatibility, biodegradability, low-cost, etc (Islam et al., 2017; Pestov and Bratskaya, 2016). Previous studies of chitosan as a stabilizing agent showed that it produces stabilized metallic (silver, gold, iron and platinum) nanoparticles with moderately average diameters (Ahmadi et al., 2017; Huang et al., 2004).

Recently different iron-based bimetallic nanoparticles were used for the removal of chlorinated organic compounds, inorganic anions and heavy metals (Bhaskar et al., 2016). Limited study has been done regarding the degradation of dyes from the aqueous solution. Most of the studies in the removal of textile dyes deal with azo dyes (Bokare et al., 2008) and only a few studies were conducted based on the degradation of triphenylmethane dyes. In our present study, the cationic triphenylmethane malachite green dye (MG) and anionic triphenylmethane methyl blue dye (MB) was used as a model pollutant as shown in Fig.1. MG dye is widely used in the textile, food and fish hatchery industries and it is environmentally persistent. The previous studies revealed that the extensive use of MG cause several health hazards in aquatic organisms and it will retard the light penetration in hydrosphere eventually affect the photosynthesis in the aquatic ecosystem (Kumar et al., 2015). MB dye is extensively used in biological and bacteriological staining and the textile industry (Hou et al., 2007). A very little study has been reported about the toxicity and removal of MB from aqueous media. Therefore it is necessary to execute proper treatments to remove the dyestuffs from wastewater before entering to the aquatic ecosystem.

In this work, we have synthesised chitosan-stabilized Fe (CS-Fe) and chitosan-stabilized Fe/Ni (CS-Fe/Ni) nanoparticles by using chitosan as a stabilizing agent for the removal of triphenylmethane dyes. We have also investigated the influence of different parameters, such as the initial dye concentration, dosage of adsorbent, contact time, pH of the dye solution and ionic strength using NaCl solution for removal of triphenylmethane dyes

2. Materials and methods

2.1. Chemicals and materials

Iron(III) chloride hexahydrate (Sigma-Aldrich, ≥99 %), Nickel(II) sulfate hexahydrate (Merck, Emsure), Sodium borohydride (Sigma-Aldrich, ≥98%), Chitosan (Sigma-Aldrich, low molecular weight), Malachite green (Nice) and Methyl Blue (Merck) were bought from the market and were used as such without further purification .

2.2. Synthesis of CS-Fe and CS-Fe/Ni bimetallic nanoparticles

Fig. 2 is a schematic representation of the synthesis of CS-Fe/Ni nanoparticles using chitosan as a stabilizer. CS-Fe and CS-Fe/Ni nanoparticles were prepared via liquid-phase reduction method using sodium borohydride as a reducing agent (Gonçalves et al., 2018; Weng et al., 2013b). Chitosan (0.5 %), the stabilizer, used for the synthesis of CS-Fe and CS-Fe/Ni nanoparticles were dissolved in dil. acetic acid through ultrasonic vibration treatment. For the synthesis of CS-Fe/Ni nanoparticles, the metal solutions of $FeCl_3.6H_2O$ (0.973 g) and

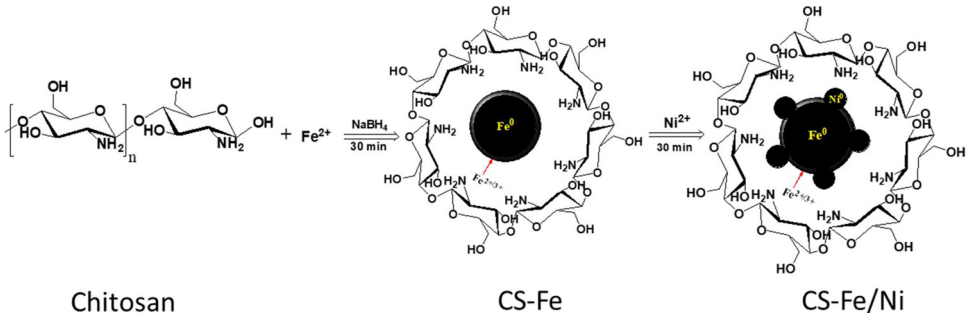

Fig. 2. Schematic representation of the synthesis of CS-Fe/Ni nanoparticles.

$NiSO_4.6H_2O$ (0.089 g) were prepared in 10 mL deionized water. The prepared $FeCl_3.6H_2O$ solution was incorporated with the dissolved chitosan solution in a round bottom flask under nitrogen atmosphere. The mixture was stirred for 15 min using a magnetic stirrer and 60 mL of NaBH4 (0.544 g) solution prepared in the ethanol-water system was added drop by drop into this mixture and stirred vigorously and continuously for 30 min. A black coloured precipitate of CS-Fe was formed as represented in Eq. (1).

$$CS + Fe^{2+} + 2BH_4^- + 6H_2O \rightarrow CS\text{-}Fe^{\circ} + 2B(OH)_3 + 7H_2 \quad (1)$$

Then $NiSO_4.6H_2O$ solution was added to CS-Fe solution and agitated for another 30 min. This would lead to the formation of CS-Fe/Ni nanoparticles which is described by Eq. (2). The prepared nanoparticles were collected through vacuum filtration and the nanoparticles were rinsed with deionized water, absolute ethanol and acetone successively. The prepared nanoparticles were lyophilized and stored in a sealed bottle.

$$CS\text{-}Fe^{\circ} + Ni^{2+} \rightarrow CS\text{-}Fe^{\circ}/Ni^{\circ} + Fe^{2+} \quad (2)$$

The method for synthesis of CS-Fe particles was similar to that of chitosan stabilized Fe/Ni nanoparticles, except that the $NiSO_4.6H_2O$ solution was not be added during the preparation of nanoparticles.

2.3. Batch experiments

Dye removal experiments were carried out in 100 mL beakers with 20 mL of dye solution of the desired concentration. The MG and MB dye solution of desired concentration were prepared by dilution of stock solution instantly before use. Firstly, 50 ppm of the dye solution was added to the beaker and rapidly mixed with the nanoparticles of a particular dosage. Then the beakers were agitated in a bath sonicator for 1 hr. The samples were collected at regular intervals whose absorbance were measured using a UV–vis spectrophotometer. Samples without the addition of nanoparticles have experimented under identical conditions and no significant changes were observed. The effects of adsorbent dosage, initial concentration of dye, pH, ionic strength and contact time were also investigated. To study the effect of pH, the initial pH of the dye solution was adjusted using 1.0 M NaOH and 1.0 M H_2SO_4. In order to investigate the influence of ionic strength, 20 mL of NaCl solution was added to 40 mL of 50 ppm dye solution and the concentration of the NaCl solution was varied from 0.001 M to 0.1 M. All samples were analysed for the residual dye concentration using UV–vis Spectrophotometer. All experiments were performed with a duplicate.

2.4. Characterisation and analytical techniques

The particle size and morphology of the CS-Fe and CS-Fe/Ni nanoparticles were analyzed by using Jeol/JEM 2100 High resolution transmission electron micrograph (HRTEM). The binding energies of CS, CS-Fe and CS-Fe/Ni nanoparticles were investigated via X-ray photoelectron spectroscopy (XPS, Kratos Analytical, Ultra axis). The FTIR spectra of CS, CS-Fe and CS-Fe/Ni nanoparticles before and after adsorption / degradation were investigated through Fourier transform infrared spectrometer (SHIMADZU IR Affinity-1) in the wavelength range of 4000 – 600 cm^{-1}. Samples for FTIR analysis were prepared by mixing KBr with the samples and pressed into small thin pellets. The prepared nanoparticles were lyophilized using Operon FDU 7003 lyophilizer. The surface charge of the prepared nanoparticles was investigated through zeta potential using Laser zeta sizer (Malvern).

The absorbance of dye solution was measured using UV–vis spectrophotometer (SHIMADZU UV 1800). Stock solutions of MB and MG were prepared in demineralized water. The absorbance of MG and MB were measured at 617 nm and 595 nm respectively. The dye removal efficiency was calculated using the eq.3 :

$$Percentage\ of\ Removal\ (\%R) = \frac{C\square - Ct}{C\square} * 100 \quad (3)$$

Where C_0 (mg/L) is initial dye concentration, and Ct (mg/L) is the concentration of dye at t min.

3. Results and discussions

3.1. Characterization of CS, CS-Fe and CS-Fe/Ni nanoparticles

3.1.1. TEM

The Transmission Electron Micrographs of the CS-Fe/Ni and CS-Fe as shown in Fig. 3 revealed that a layer of grey material was covering on the spherical metallic nanoparticle. This was similar to the core-shell structure of a nanoparticle. As the chitosan was used as a stabilizer, it was assumed that Fe° core would have been coated with a layer of chitosan as the shell. By randomly counting around 50 nanoparticles in the TEM photograph, the average diameter of the CS-Fe and CS-Fe/Ni nanoparticles were estimated as 14.87 nm and 9.2 nm with a metallic core of 9.73 nm and 5.57 nm respectively. It is believed that the chitosan reduced the agglomeration tendency of nanoparticles arose from the magnetic property of iron nanoparticle and protects the iron nanoparticle from oxidation by binding Fe° with hydroxyl and amine groups of the chitosan (Geng et al., 2009).

3.1.2. XPS

The composition of the nanoparticles and oxidation states of elements in the nanoparticles was analyzed by X-ray Photoelectron Spectroscopy (XPS). Being a surface analyzing technique, XPS can investigate only up to 5−10 nm depth of the sample (Gerber and Erasmus, 2018). XPS wide scan spectra of CS, CS-Fe and CS-Fe/Ni are shown in Fig. 4. From this spectra, it was evident that C, N, O, Fe and Ni were the elements mainly present in CS-Fe/Ni nanoparticles. They also contained small amounts of elements B and Na, which were reaction residue from the preparation of nanoparticles. Compared with the parent CS, the main difference between CS-Fe/Ni and CS-Fe were the emergence of photoelectron peaks of Fe and Ni in CS-Fe/Ni and Fe in CS-Fe nanoparticles. Even though the intensity of N 1s was more

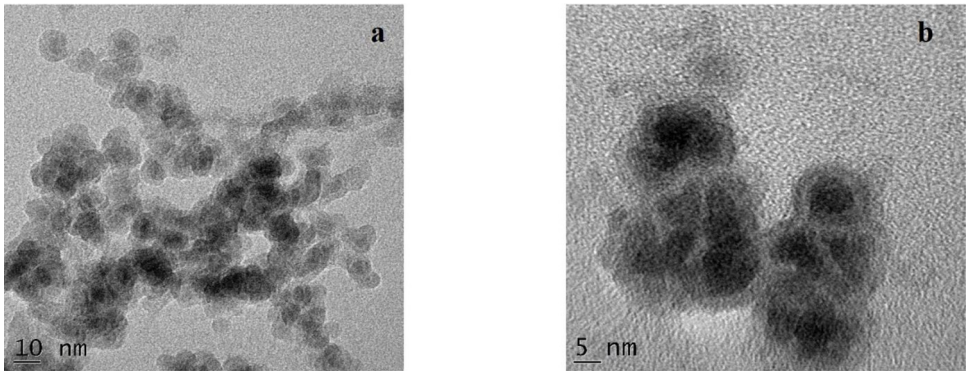

Fig. 3. HRTEM image of (a) CS-Fe/Ni and (b) CS-Fe nanoparticles.

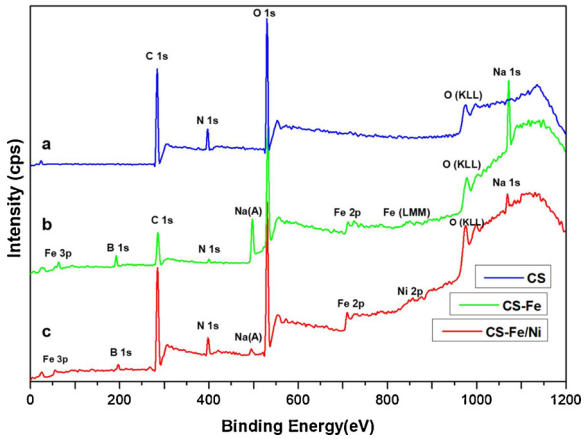

Fig. 4. XPS wide scan survey of (a) CS, (b) CS-Fe and (c) CS-Fe/Ni nanoparticles.

predominant in CS, a decrease in intensity in N 1s photoelectron peak was observed in CS-Fe and CS-Fe/Ni, this may be due to complexation of N 1s with iron nanoparticles.

A comparison of Fe 2 P region spectra of CS-Fe and CS-Fe/Ni nanoparticles and Ni 2 P region spectra of CS-Fe/Ni nanoparticles were as shown in Fig. 5. The existence of zero valent iron was confirmed by photoelectron peak around 708.05 eV and 720.95 eV which corresponds to the $2p^{3/2}$ and $2p^{1/2}$ binding energies of Fe° in CS-Fe/Ni nanoparticles (Desalegn et al., 2019; Momose et al., 2016). The predominant photoelectron peak of CS-Fe/Ni at 709.55 eV and 722.15 eV matched with the binding energies of $2p^{3/2}$ and $2p^{1/2}$ of Fe^{2+} in FeO (Xie et al., 2016). The results revealed that the CS-Fe/Ni nanoparticles were covered with a thin shell of iron oxide, mainly FeO. The detailed Fe 2 P spectrum of the surface of CS-Fe nanoparticles mainly consists of Fe^{3+} species which was indicated by the major photoelectron peak around 711.55 eV and 725.55 eV which belonged to the binding energies of $2p^{3/2}$ and $2p^{1/2}$ of Fe^{3+} respectively (Geng et al., 2009). As compared with the CS-Fe/Ni, photoelectron line around 708.05 eV and 720.85 eV was less in CS-Fe which indicated that more metallic iron was oxidized in CS-Fe. The Fe^{3+} species in samples may be due to the presence of FeOOH, Fe_3O_4, Fe_2O_3 or Fe^{3+} – chitosan complex. The oxidation of iron occurred during the detection process resulted in the high intensity of Fe^{3+} photoelectron peaks of the samples. The Ni 2 P detailed spectra in CS-Fe/Ni was complex due to the interaction between iron and chitosan. The photoelectron peak at 853.7 eV and 872.35 eV corresponded to the $2p^{3/2}$ and $2p^{1/2}$ binding energies of Ni^{2+} respectively in CS-Fe/Ni nanoparticles (Huang et al., 2017). This may be due to the oxidation of Ni on the surface of Fe°.

3.1.3. Zeta potential

The surface charge of CS, CS-Fe and CS-Fe/Ni was studied by measuring zeta potential which gives valuable information about the interaction between adsorbent and adsorbate. The zeta potential of CS, CS-Fe and CS-Fe/Ni nanoparticles were found negative with values of -2.1 mV, -8.5 mV and -3.1 mV respectively in aqueous medium as shown in Fig. S4. The pH of the medium is alkaline due to the formation of hydroxyl ion as a result of the reaction between iron nanoparticle and water. To impart more stability, the nanoparticle are encapsulated within the chitosan matrix. The negative charge of zeta potential comes from the negatively charged hydroxide groups on the chitosan matrix (Adeyi et al., 2019). The zeta potential of the CS-Fe and CS-Fe/Ni nanoparticles matched with the zeta potential of chitosan in water.

3.2. Dye removal studies using CS-Fe and CS-Fe/Ni nanoparticles

3.2.1. UV–vis spectrophotometric analysis

The MG and MB dye removal efficiency were studied using CS, CS-Fe and CS-Fe/Ni nanoparticles through UV–vis spectroscopy as shown in Fig. 6. The initial pH of MG and MB dye solution was 3.6 and 5.0 respectively without pH adjustment.. The addition of CS-Fe and CS-Fe/Ni nanoparticles changed the pH to alkaline due to the iron corrosion and formation of hydroxyl ion when reacting with water. The pH of the dye solution was changed into around 9.2 in MG and MB after adding

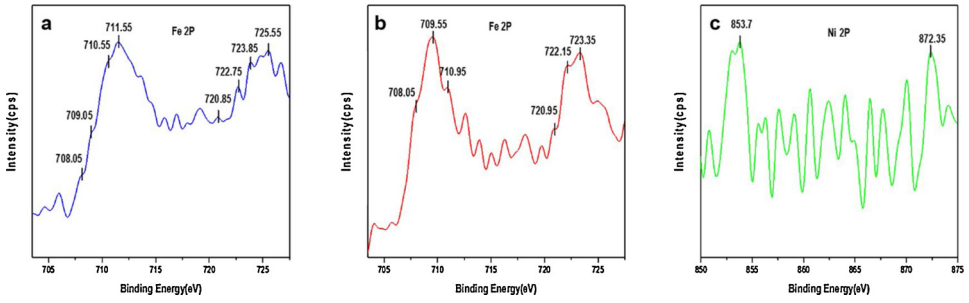

Fig. 5. Detailed XPS spectra of (a) Fe 2 P in CS-Fe and (b) Fe 2p and (c) Ni 2 P in CS-Fe/Ni.

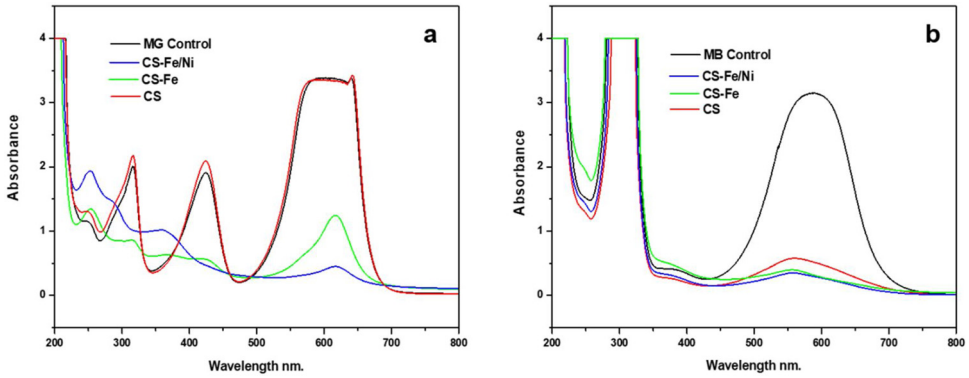

Fig. 6. UV–vis spectra of removal of (a) MG and (b) MB dye using CS, CS-Fe and CS-Fe/Ni nanoparticles.

the CS-Fe and CS-Fe/Ni nanoparticles. In the case of MG, the major absorption peak of MG appeared at 617 nm which corresponded to the functional group, -C = C- and C = N-, of MG. The peaks at 425 nm, 315 nm and 250 nm could be assigned to the aromatic rings and conjugated chromophore of MG (Wang et al., 2017; Weng et al., 2013a). The results show that the peaks at 617 nm, 425 nm and 315 nm were alarmingly decreased in CS-Fe and CS-Fe/Ni nanoparticles containing dye solution within 60 min and the chitosan does not influence the degradation of MG. The sharp decrease in the 617 nm peak indicates that the decolourization of MG occurred mainly due to the cleavage of the functional group of MG. The conjugated chromophore structure of MG would also be completely demolished or adsorbed by the CS-Fe and CS-Fe/Ni nanoparticles simultaneously which was indicated by the absence of a peak at 425 nm. The emergence of new peaks centred at around 360 nm as a degradation product also supported the previous assumption that the removal of MG was through degradation and adsorption (He et al., 2012). Regarding the removal of MB, the CS, CS-Fe and CS-Fe/Ni nanoparticles showed high dye decolourisation efficiency which could be due to its better adsorptive capacity. The characteristic peak of MB observed at 595 nm (Wang et al., 2015) shifted towards lower wavelength due to its interaction with nanoparticles and chitosan, leading to a change in the pH of the dye solution. No new peaks emerged as a consequence of MB dye removal using CS, CS-Fe and CS-Fe/Ni nanoparticles which indicated that the removal of MB occurred through the adsorption process.

The dye removal mechanism of prepared nanoparticles and chitosan was through the degradation catalysed by Fe° and adsorption caused by iron oxide shell and chitosan. The Fe° nanoparticles destroy chromophore of the dye molecule through atomic hydrogen which was produced by the reaction between Fe° and H_2O and H^+ (He et al., 2012). Ni on the surface of Fe° acted as a catalyst which facilitated atomic hydrogen production and enabled the electron transfer through the iron oxide shell. This stimulated the Fe/Ni nanoparticle for a greater dye removal efficiency (Bokare et al., 2008). As stabilizer chitosan not only protect the iron nanoparticles and increase the interaction between Fe° and dye but also show a synergetic effect on the dye removal through adsorption. In this study, CS-Fe/Ni nanoparticle showed a higher dye removal efficiency compared to the CS-Fe nanoparticles which were consistent with the previous assumptions (Weng et al., 2013b).

3.2.2. FTIR spectra

The FTIR analysis spectrum of CS, CS-Fe and CS-Fe/Ni nanoparticles were as shown in Fig. 7. The FTIR measurements were carried out to determine the possible interactions between the metallic nanoparticle and chitosan. A broad overlapping band of OH stretching and N—H stretching of amine in chitosan was observed in the region centered at 3354 cm^{-1}. The absorption band at 2875 cm^{-1} was attributed to the C–H stretching vibrations. The absorption appeared at 1643 cm^{-1} corresponded to the C== O stretching of amide. The N—H bending

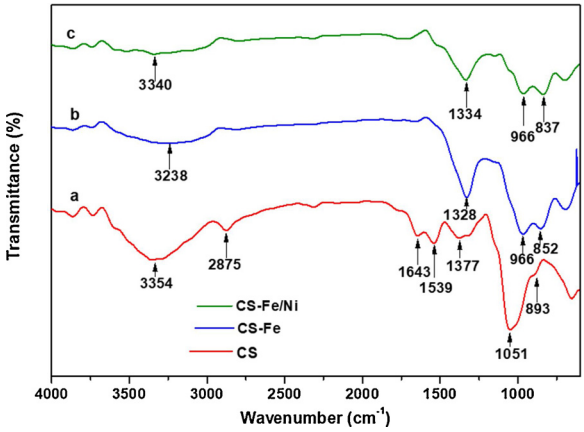

Fig. 7. FTIR spectra of (a) CS, (b) CS-Fe and (c) CS-Fe/Ni nanoparticles.

vibration of the 1° amines was displayed by the absorption peak at 1539 cm^{-1}. The band at 1377 cm^{-1} corresponds to the bending vibrations of O—H and deformation of $-CH_3$ and $-CH_2$. Absorption peak observed at 1051 cm^{-1} could be due to the stretching vibrations of C—O (1° alcohol)/ COC / CN———(1° amine). The peak at 893 cm^{-1} corresponded to the bending vibrations of = CH and = CH_2 (Geng et al., 2009; Jiang et al., 2018; Weng et al., 2013b).

The FTIR spectrum of CS-Fe and CS-Fe/Ni was different compared to the spectrum of chitosan. The broad bands corresponding to O—H and NH— stretching of amine in chitosan was weakened and shifted to lower wavenumber in CS-Fe and CS-Fe/Ni. This may be due to the interaction of iron nanoparticles with these groups of chitosan. In addition to that, the intensity of peaks at 2875,1643 and 1539 cm^{-1} decreased entirely and peaks at 1377, 1051 and 893 cm^{-1} shifted to lower wavenumber. From these results, it could be concluded that the iron interacted with amine and hydroxyl functional groups of chitosan which proved to be a versatile stabilizer for zero valent iron. Addition of second metal, Ni, possessed less significant changes in the IR spectra of CS-Fe/Ni compared with CS-Fe. This may be due to the low percentage of Ni in CS-Fe/Ni nanoparticles (Jiang et al., 2018; Weng et al., 2013b).

FTIR spectra of CS, CS-Fe and CS-Fe/Ni nanoparticles showed remarkable changes after the adsorption and/or degradation of MB and MG dyes. The pattern of the fingerprint region changed due to the interaction between the prepared nanoparticles and dyes. Fig. 8(a,b) shown the FTIR spectra of CS-Fe/Ni nanoparticles after the adsorption/ degradation of MG and MB respectively. In the case of parent MG dye, the specific peaks in the fingerprint region (500 − 1500 cm^{-1}) matched to the mono-substituted and para-disubstituted benzene rings which are due to the C = C stretching of the benzene ring seen at 1576 cm=$^{-1}$. MG also showed peaks at 1157 cm^{-1} and 1221 cm^{-1} corresponds to C-

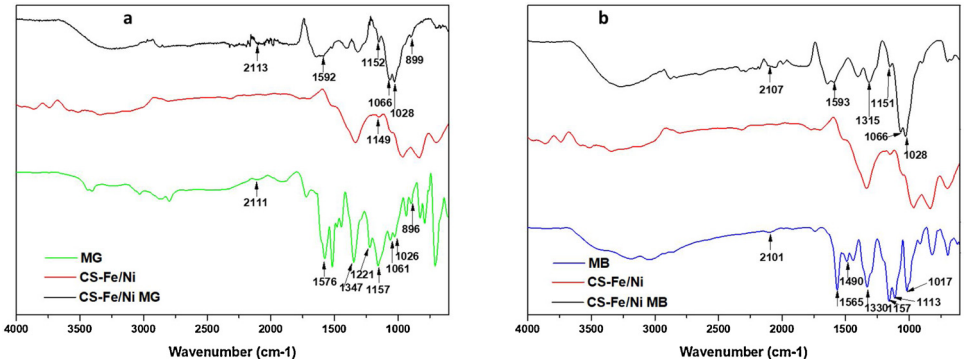

Fig. 8. FTIR spectra of CS-Fe/Ni nanoparticles after the removal of MG (a) and MB (b).

N stretching vibrations (−Bhagavathi Pushpa et al., 2015). The peaks of parent MG dye are also seen in CS-Fe/Ni nanoparticles after adsorption of MG. Some of the IR peaks of MG gets vanished which indicates the destruction of the structure of the MG. The CS-Fe/Ni nanoparticles after treated with dye showed a similar peak of C=C stretching at 1592 cm=$^{-1}$. The absence of peaks between (850 – 670 cm^{-1}) supported the total disappearance of aromatic rings of MG in prepared nanoparticles. The peaks at 1221 cm^{-1} and 1347 cm^{-1} corresponded to the C-N stretching and C–H bending which was also absent in the CS-Fe/Ni nanoparticles after MG degradation (−Raizada et al., 2014). This indicates that removal of MG through CS-Fe/Ni nanoparticles changed the structure of MG. MG removal through CS and CS-Fe (Fig. S5) also showed a similar pattern of changes as CS-Fe//Ni nanoparticles except CS has some more peaks similar to MG. This indicates that the removal of MG through CS mainly through adsorption.

In the case of parent MB, the bands at the 1565 cm^{-1} was corresponding to NH stretching vibrations, the peaks occurred at 1113−1490 cm−$^{-1}$ were belonged to the framework vibration of benzene rings. The peak observed at 1017 cm^{-1} can be assigned to the S=O stretching vibrations (=Yang et al., 2014). The FTIR spectra of CS-Fe/Ni nanoparticles after adsorption of MB showed the similar peaks of parent MB dye which indicates that some of the MB molecules are adsorbed onto the CS-Fe/Ni nanoparticles. The MB peaks seen in CS-Fe/Ni nanoparticles show a shift into lower wavenumber and some of the peaks are absent too. This suggests the destruction of the methyl blue structure by CS-Fe/Ni nanoparticles. The peaks of the CS-Fe nanoparticle after MB adsorption (Fig. S6 a) is similar to that of CS-Fe/Ni nanoparticles. But in the case of CS after MB adsorption (Fig. S6 b), more peaks are similar to parent MB dye compared with CS-Fe and CS-Fe/Ni nanoparticles. This indicates that MB removal through CS is mainly by adsorption.

3.3. Effects of parameters on the removal of MG and MB

3.3.1. Effect of the initial concentration

The effect of the initial concentration of MG and MB dye was investigated in 20 mL of different dye concentration ranging from 50 to 150 mg/L by using 2 g/L of CS, CS-Fe and CS-Fe/Ni nanoparticles as shown in Fig. 9. The highest removal efficiencies of CS, CS-Fe and CS-Fe/Ni nanoparticles were 19 %, 88 % and 94 % respectively for MG and 74 %, 83 % and 85 % for MB at 50 mg/L of dye solution. The removal efficiencies seemed to be decreasing with the increase in the initial concentration of the dyes. It was considered that removal of MG through CS-Fe and CS-Fe/Ni was a heterogeneous reaction which is greatly influenced by adsorption and degradation through Fe and chitosan. But the removal of MB was only through the adsorption of prepared nanoparticles and chitosan. When the initial concentration of dye increased, competitive adsorption was established between the dye molecule and a fixed dosage of adsorbent and this eventually led to the decline in dye removal efficiency of CS, CS-Fe and CS-Fe/Ni nanoparticles.

3.3.2. Effect of dosage of adsorbent

The effect of dosage of adsorbent was studied in 4 different adsorbent dosage, 0.5 g/L, 1 g/L, 1.5 g/L and 2 g/L on 50 mg/L of 40 mL dye solution are showed in Fig. 10. The highest removal efficiency, 94 % for MG and 82 % for MB were seen in CS-Fe/Ni at 2 g/L. These results highlighted the fact that the increase in dosage of CS-Fe and CS-Fe/Ni nanoparticles boost the removal efficiency of MG and MB to a large extent. This was similar to the previous studies of dye removal using iron nanoparticles (Guo et al., 2012). In the case of MB, chitosan also showed a high removal efficiency as a consequence of the adsorptive property of chitosan as a cationic polymer (Lin et al., 2014). It is a well-known fact that the dye removal efficiency was greatly influenced by the concentration of available active reactive sites of Fe (Wang et al., 2015). The increase in dosage of CS-Fe and CS-Fe/Ni nanoparticles with a small particles size would increase the total surface adsorptive sites available for dye degradation / adsorption which eventually lead to a higher dye removal efficiency of MG and MB.

3.3.3. Effect of contact time

Fig. 11 demonstrates the effect of contact time on the MG and MB dye removal at the 50 mg/L of dye solution of 40 mL using 2 g/L of the adsorbent. The removal efficiency of MG and MB dye were studied at 3 different time intervals of 60 min. 99 % and 88 % dye removal for MG and MB respectively were obtained by CS-Fe/Ni nanoparticles within 180 min. The results showed that first 60 min exhibit a greater removal efficiency for MG and MB dye in CS-Fe and CS-Fe/Ni nanoparticles. The chitosan showed a 77 % dye removal for MB in 180 min. This may be due to the presence of tremendous empty active sites on the surface of Fe and chitosan primarily. As the dye molecules were adsorbed onto the Fe surface and chitosan, the availability of active adsorptive sites decreased gradually which lead to the decrease in the rate of removal efficiency in MG and MB dye with time.

3.3.4. Effect of PH

The influence of pH on the MG and MB dye removal was studied at pH 4, pH 8 and pH 12 of 50 ppm dye solution as shown in Fig. 12. The fading of triphenylmethane dyes (MB and MG) is due to the hydroxide ion attack on the central C atom of the planar ring system and in a way obstructing its conjugation orientation (Felix, 2017). The dyes become colourless at pH 12. The dye removal studies reveal that the highest removal efficiency for MG and MB took place in acidic pH with 89 % dye removal for both MG and MB. The removal of MB and MG dye decreased with the increase in pH of the solution. This is attributed to the hydroxide precipitation at the surface of iron nanoparticles at alkaline pH (Huang et al., 2015) and this eventually leads to the decrease in reactivity of CS-Fe and CS-Fe/Ni nanoparticles. From the above observation, it could also be concluded that simple adsorption takes place at higher pH. As the pH decreases, the depletion of iron oxide shell, as

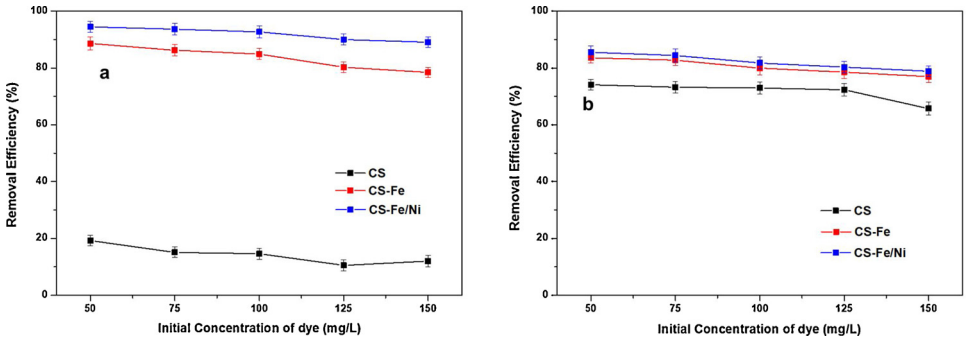

Fig. 9. Effect of initial (a) MG and (b) MB dye concentration on dye removal.

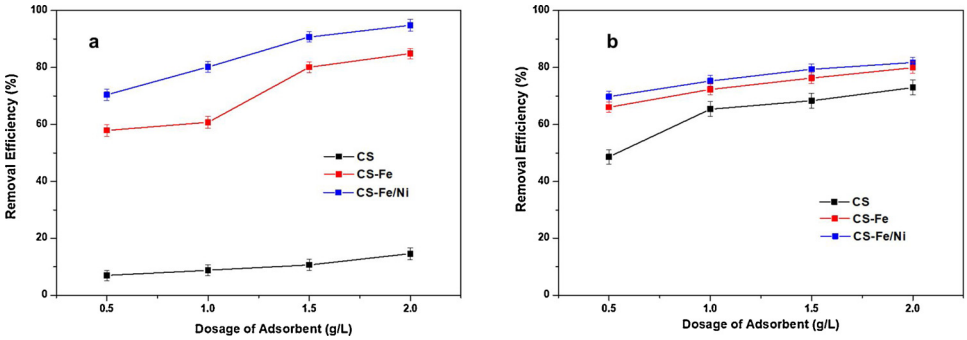

Fig. 10. Effect of dosage of adsorbent in (a) MG and (b) MB dye removal.

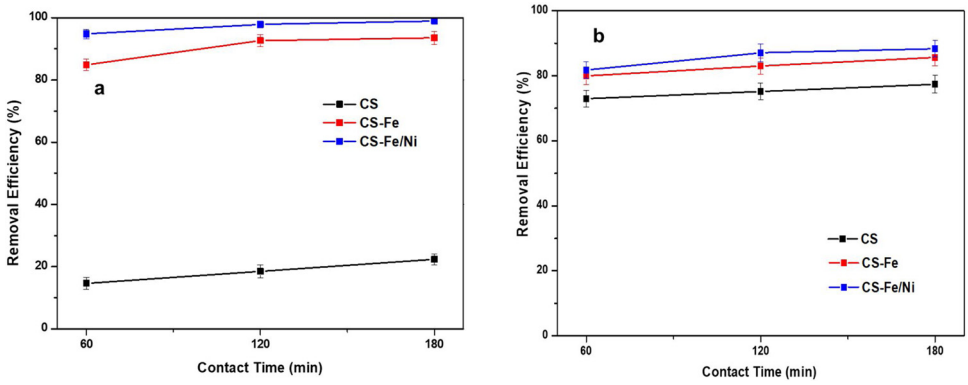

Fig. 11. Effect of contact time in (a) MG and (b) MB dye removal.

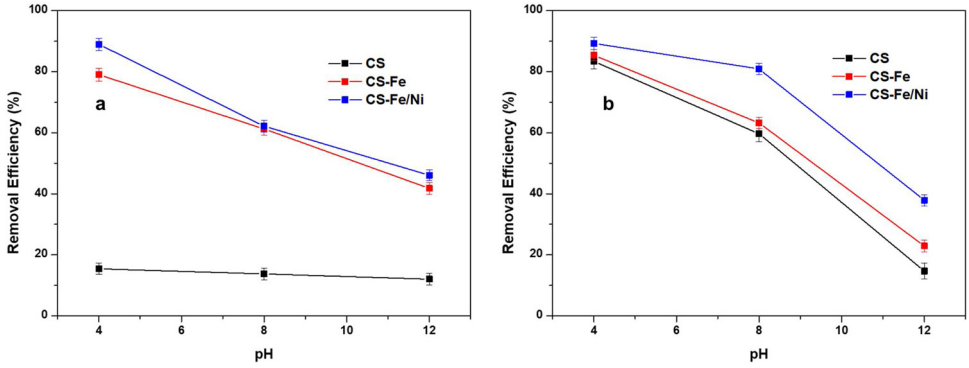

Fig. 12. Effect of pH in (a) MG and (b) MB dye removal.

well as solubilization of chitosan, takes place exposing inner Fe° core. Due to this, cleavage of -C = C- and -C = N- bonds take place in addition to adsorption (Freyria et al., 2017). This leads to the more availability of iron nanoparticles for adsorption and degradation.

3.3.5. *Effect of ionic strength*

The effect of ionic strength was studied through the addition of NaCl to the dye solution as shown in Fig. 13. The influence of ionic strength is studied in three different NaCl concentration of 0.001 M, 0.01 M and

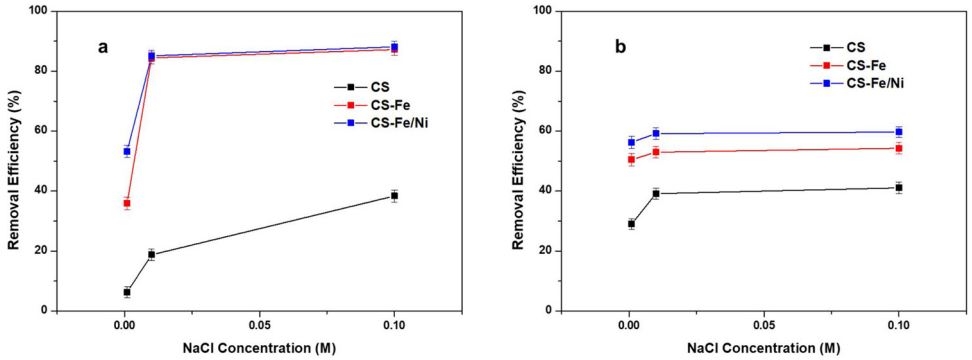

Fig. 13. Effect of ionic strength in (a) MG and (b) MB dye removal.

0.1 M. In the case of ions that form outer-sphere surface complexes, the rise in ionic strength leads to a decrease in adsorption. But in the case of inner-sphere surface complexes, they show increasing adsorption with increasing ionic strength (Anirudhan and Ramachandran, 2007). The introduction of the NaCl solution to the iron nanoparticles makes multiple effects on dye removal. When the NaCl concentration increases, the iron oxide shell drained away by reacting with the chloride ion. This will rejuvenate the Fe° surface and enhance dye degradation in large extent. The results show that the introduction of NaCl decreases the MB dye removal, even though there is a negligible effect on MB adsorption with increasing ionic strength. These results indicate that the negatively charged Cl^- ions form a wall around the CS-Fe/Ni nanoparticles. Due to this, the methyl blue molecules cannot reach the nanoparticle surface and eventually leads to a decrease in decolourisation (Taylor et al., 2015). This results also show that MB removal was through both outer-sphere surface complexes and destruction of the conjugated structure of dye molecule by inner Fe°core (Mahmoud et al., 2016; Yu et al., 2019). In the case of MG, there is no significant decrease in dye removal with increasing ionic strength. This will indicate that the removal of MG mainly through cleavage functional groups compared with adsorption to the iron oxide shell.

4. Conclusion

The bimetallic Fe/Ni nanoparticles stabilized on the biopolymer chitosan (CS-Fe/Ni) provided quicker MG and MB dye removal compared with monometallic Fe stabilized chitosan (CS-Fe) and the chitosan (CS). The cationic polymer, CS, exhibited a high removal efficiency for anionic dye MB, which corresponded to the adsorptive property of the chitosan. The greater dye removal efficiency of CS-Fe/Ni nanoparticle was credited to the small size of prepared nanoparticles and catalytic property of second metal Ni. In addition to this, the effect of different parameters in the removal process of MB and MG were displayed by the prepared nanoparticles. The low initial concentration of dye was a favourable condition for the high removal efficiency of prepared nanoparticles. In general, the prepared CS-Fe/Ni nanoparticles look more suitable for the removal of MG compared to the MB dye.

CRediT authorship contribution statement

Anju Rose Puthukkara P.: Conceptualization, Methodology, Software, Data curation, Writing - original draft. **Sunil Jose T.:** Supervision. **Dinoop lal S.:** Software, Writing - review & editing.

Declaration of Competing Interest

None.

Acknowledgements

The financial support of the “KSCSTE Research Fellowship” from Kerala State Council for Science, Technology and Environment,Kerala, Indiais gratefully acknowledged.

References

Adeyi, A.A., Jamil, S.N.A.M., Abdullah, L.C., Choong, T.S.Y., 2019. Adsorption of Malachite Green Dye From Liquid Phase Using Hydrophilic Thiourea-modified Poly (acrylonitrile- Co -acrylic Acid): Kinetic and Isotherm Studies. 2019. .

Adusei-Gyamfi, J., Acha, V., 2016. Carriers for nano zerovalent iron (nZVI): synthesis, application and efficiency. RSC Adv. 6, 91025–91044. https://doi.org/10.1039/c6ra16657a.

Ahmadi, M., Foladivanda, M., Jafarzadeh, N., Ramavandi, B., Kakavandi, B., 2017. https://doi.org/10.2166/aqua.2017.027.

Amin, M.T., Alazba, A.A., Manzoor, U., 2014. A review of removal of pollutants from water/wastewater using different types of nanomaterials. Adv. Mater. Sci. Eng. 2014. https://doi.org/10.1155/2014/825910.

Anirudhan, T.S., Ramachandran, M., 2007. Surfactant-Modified Bentonite as Adsorbent for the Removal of Humic Acid from Wastewaters 35. pp. 276–281. https://doi.org/10.1016/j.clay.2006.09.009.

Batool, S., Akib, S., Ahmad, M., Balkhair, K.S., Ashraf, M.A., 2014. Study of Modern Nano Enhanced Techniques for Removal of Dyes and Metals. 2014. .

Bhagavathi Pushpa, T., Vijayaraghavan, J., Sardhar Basha, S.J., Sekaran, V., Vijayaraghavan, K., Jegan, J., 2015. Investigation on removal of malachite green using EM based compost as adsorbent. Ecotoxicol. Environ. Saf. 118, 177–182. https://doi.org/10.1016/j.ecoenv.2015.04.033.

Bhaskar, A.V., Jaafar, J., Manohara, Y.V., Bin, A., Abdul, Z., Talib, J., Madhavi, G., 2016. Journal of Environmental Chemical Engineering Recent Progress on Fe-Based Nanoparticles : Synthesis, Properties, Characterization and Environmental Applications 4. pp. 3537–3553. https://doi.org/10.1016/j.jece.2016.07.035.

Bokare, A.D., Chikate, R.C., Rode, C.V., Paknikar, K.M., 2008. Iron-Nickel Bimetallic Nanoparticles for Reductive Degradation of Azo Dye Orange G in Aqueous Solution 79. pp. 270–278. https://doi.org/10.1016/j.apcatb.2007.10.033.

Desalegn, B., Megharaj, M., Chen, Z., Naidu, R., 2019. Heliyon Green synthesis of zero valent iron nanoparticle using mango peel extract and surface characterization using XPS and GC-MS. Heliyon 5, e01750. https://doi.org/10.1016/j.heliyon.2019.e01750.

Ezzatahmadi, N., Marshall, D.L., Hou, K., Ayoko, G.A., Millar, G.J., Xi, Y., 2019. Simultaneous adsorption and degradation of 2,4-dichlorophenol on sepiolite-supported bimetallic Fe/Ni nanoparticles. J. Environ. Chem. Eng. 7, 102955. https://doi.org/10.1016/j.jece.2019.102955.

Felix, L.D., 2017. Kinetics of the reaction between malachite green and hydroxyl ion in the presence of reducing sugars. Latona Dayo Felix 526–531.

Foster, S.L., Estoque, K., Voecks, M., Rentz, N., Greenlee, L.F., 2019. Removal of synthetic azo dye using bimetallic nickel-iron nanoparticles. J. Nanomater. 2019. https://doi.org/10.1155/2019/9807605.

Freyria, F.S., Esposito, S., Armandi, M., Deorsola, F., Garrone, E., Bonelli, B., 2017. Role of pH in the Aqueous Phase Reactivity of Zerovalent Iron nanoparticles With Acid Orange 7, A Model Molecule of Azo Dyes. 2017. .

Fu, F., Dionysiou, D.D., Liu, H., 2014. The use of zero-valent iron for groundwater remediation and wastewater treatment: a review. J. Hazard. Mater. 267, 194–205. https://doi.org/10.1016/j.jhazmat.2013.12.062.

Gao, Y., Wang, F., Wu, Y., Naidu, R., Chen, Z., 2016. Comparison of degradation mechanisms of microcystin-LR using nanoscale zero-valent iron (nZVI) and bimetallic Fe/Ni and Fe/Pd nanoparticles. Chem. Eng. J. 285, 459–466. https://doi.org/10.1016/j.cej.2015.09.078.

Geng, B., Jin, Z., Li, T., Qi, X., 2009. Preparation of chitosan-stabilized Fe 0 nanoparticles for removal of hexavalent chromium in water. Sci. Total Environ. 407, 4994–5000. https://doi.org/10.1016/j.scitotenv.2009.05.051.

Gerber, S.J., Erasmus, E., 2018. Electronic effects of metal hexacyanoferrates : an XPS and FTIR study. Mater. Chem. Phys. 203, 73–81. https://doi.org/10.1016/j.

matchemphys.2017.09.029.
Gonçalves, A.A., Araújo, A.F., José, M., Pires, M., Moreira, R., 2018. Synthesis of Chitosan-stabilised Iron and Nickel Nanoparticles and the Application in the Reductive Degradation of Nimesulide. https://doi.org/10.26850/1678-4618eqj.v43.1.10-25.
Guo, J., Wang, R., Tjiu, W.W., Pan, J., Liu, T., 2012. Synthesis of Fe nanoparticles@ graphene composites for environmental applications. J. Hazard. Mater. 225–226, 63–73. https://doi.org/10.1016/j.jhazmat.2012.04.065.
He, Y., Gao, J.F., Feng, F.Q., Liu, C., Peng, Y.Z., Wang, S.Y., 2012. The comparative study on the rapid decolorization of azo, anthraquinone and triphenylmethane dyes by zero-valent iron. Chem. Eng. J. 179, 8–18. https://doi.org/10.1016/j.cej.2011.05.107.
Hou, X., Tong, X., Dong, W., Dong, C., Shuang, S., 2007. Synchronous Fluorescence Determination of Human serum Albumin With Methyl Blue as a Fluorescence Probe 66. pp. 552–556. https://doi.org/10.1016/j.saa.2006.03.031.
Huang, H., Yuan, Q., Yang, X., 2004. Preparation and Characterization of Metal – Chitosan Nanocomposites 39. pp. 31–37. https://doi.org/10.1016/j.colsurfb.2004.08.014.
Huang, L., Luo, F., Chen, Z., Megharaj, M., Naidu, R., 2015. Molecular and biomolecular spectroscopy green synthesized conditions impacting on the reactivity of Fe NPs for the degradation of malachite green. Spectrochim. Acta Part A Mol. Biomol. Spectrosc. 137, 154–159. https://doi.org/10.1016/j.saa.2014.08.116.
Huang, W., Ding, S., Chen, Y., Hao, W., Lai, X., Peng, J., Tu, J., Cao, Y., Li, X., 2017. 3D NiO hollow sphere/reduced graphene oxide composite for high-performance glucose biosensor. Sci. Rep. 7, 1–11. https://doi.org/10.1038/s41598-017-05528-1.
Islam, S., Bhuiyan, M.A.R., Islam, M.N., 2017. Chitin and chitosan: structure, properties and applications in biomedical engineering. J. Polym. Environ. 25, 854–866. https://doi.org/10.1007/s10924-016-0865-5.
Jiang, D., Huang, D., Lai, C., Xu, P., Zeng, G., Wan, J., Tang, L., Dong, H., Huang, B., Hu, T., 2018. Difunctional chitosan-stabilized Fe/Cu bimetallic nanoparticles for removal of hexavalent chromium wastewater. Sci. Total Environ. 644, 1181–1189. https://doi.org/10.1016/j.scitotenv.2018.06.367.
Kumar, R., Rawat, V., Banerjee, S., Angeles, M., Soni, S., Singh, S.K., Chandra, M., 2015. Synthesis of bimetallic Fe – Zn nanoparticles and its application towards adsorptive removal of carcinogenic dye malachite green and Congo red in water. J. Mol. Liq. 212, 227–236. https://doi.org/10.1016/j.molliq.2015.09.006.
Li, L., Fan, M., Brown, R., Leeuwen, J., Wang, J., Wang, W., Song, Y., Zhang, P., 2006. Synthesis, properties and environmental applications of nanoscale iron-based materials: a review. Comments Inorg. Chem. 27, 1–32. https://doi.org/10.1080/02603590500496721.
Lin, S., Chang, C., Chang, J., Mammel, K., 2014. Comparison of Dye Adsorption of Three Forms of Chitosan. pp. 319–326.
Liu, W.J., Qian, T.T., Jiang, H., 2014. Bimetallic Fe nanoparticles: recent advances in synthesis and application in catalytic elimination of environmental pollutants. Chem. Eng. J. 236, 448–463. https://doi.org/10.1016/j.cej.2013.10.062.
Mahmoud, D., Martine, W., Alexandra, M., Baudu, K.M., 2016. Phosphate removal from aqueous solutions using Zero Valent Iron (ZVI): influence of solution composition and ZVI aging. Colloids Surf. A Physicochem. Eng. Asp. https://doi.org/10.1016/j.colsurfa.2016.11.014.
Momose, Y., Tsuruya, K., Nakayama, K., 2016. Photoelectron Emission and XPS Studies of Real Iron Surfaces Subjected to Scratching in Air, Water, and Organic Liquids. pp. 202–211. https://doi.org/10.1002/sia.5942.
Pestov, A., Bratskaya, S., 2016. Chitosan and its derivatives as highly efficient polymer ligands. Molecules 21. https://doi.org/10.3390/molecules21030330.
Raizada, P., Singh, P., Kumar, A., Pare, B., Jonnalagadda, S.B., 2014. Zero valent iron-brick grain nanocomposite for enhanced solar-Fenton removal of malachite green. Sep. Purif. Technol. 133, 429–437. https://doi.org/10.1016/j.seppur.2014.07.012.
Raman, C.D., Kanmani, S., 2016. Textile dye degradation using nano zero valent iron: a review. J. Environ. Manage. 177, 341–355. https://doi.org/10.1016/j.jenvman.2016.04.034.
Raychoudhury, T., Scheytt, T., 2013. Potential of Zerovalent iron nanoparticles for remediation of environmental organic contaminants in water: a review. Water Sci. Technol. 68, 1425–1439. https://doi.org/10.2166/wst.2013.358.
Sharma, G., Kumar, A., Sharma, S., Naushad, M., Prakash Dwivedi, R., ALOthman, Z.A., Mola, G.T., 2017. Novel development of nanoparticles to bimetallic nanoparticles and their composites: a review. J. King Saud Univ. - Sci. https://doi.org/10.1016/j.jksus.2017.06.012.
Taylor, P., Sahoo, C., Gupta, A.K., 2015. Photocatalytic degradation of methyl blue by silver ion- doped titania: identification of degradation products by Photocatalytic degradation of methyl blue by silver ion-doped titania : Identi fi cation of degradation products by GC-MS and IC analysis. J. Environ. Sci. Health, Part A: Toxic/ Hazard. Substances Environ. https://doi.org/10.1080/10934529.2015.1059107.
Tesh, S.J., Scott, T.B., 2014. Nano-composites for water remediation: a review. Adv. Mater. 26, 6056–6068. https://doi.org/10.1002/adma.201401376.
Wang, X., Wang, P., Ma, J., Liu, H., Ning, P., 2015. Synthesis, characterization, and reactivity of cellulose modified nano zero-valent iron for dye discoloration. Appl. Surf. Sci. 345, 57–66. https://doi.org/10.1016/j.apsusc.2015.03.131.
Wang, X., Wang, A., Ma, J., Fu, M., 2017. Facile green synthesis of functional nanoscale zero-valent iron and studies of its activity toward ultrasound-enhanced decolorization of cationic dyes. Chemosphere 166, 80–88. https://doi.org/10.1016/j.chemosphere.2016.09.056.
Weng, X., Huang, L., Chen, Z., Megharaj, M., Naidu, R., 2013a. Synthesis of iron-based nanoparticles by green tea extract and their degradation of malachite. Ind. Crops Prod. 51, 342–347. https://doi.org/10.1016/j.indcrop.2013.09.024.
Weng, X., Lin, S., Zhong, Y., Chen, Z., 2013b. Chitosan stabilized bimetallic Fe / Ni nanoparticles used to remove mixed contaminants-amoxicillin and Cd (II) from aqueous solutions. Chem. Eng. J. 229, 27–34. https://doi.org/10.1016/j.cej.2013.05.096.
Weng, X., Chen, Zhengxian, Chen, Zuliang, Megharaj, M., Naidu, R., 2014. Clay supported bimetallic Fe/Ni nanoparticles used for reductive degradation of amoxicillin in aqueous solution: characterization and kinetics. Colloids Surf. A Physicochem. Eng. Asp. 443, 404–409. https://doi.org/10.1016/j.colsurfa.2013.11.047.
Xie, Y., Yi, Y., Qin, Y., Wang, L., Liu, G., Wu, Y., Diao, Z., 2016. Perchlorate Degradation in Aqueous Solution Using Chitosan-Stabilized Zero-Valent Iron Nanoparticles 171. pp. 164–173. https://doi.org/10.1016/j.seppur.2016.07.023.
Yan, W., Lien, H.L., Koel, B.E., Zhang, W.X., 2013. Iron nanoparticles for environmental clean-up: recent developments and future outlook. Environ. Sci. Process. Impacts 15, 63–77. https://doi.org/10.1039/c2em30691c.
Yang, X., Wang, Z., Jing, M., Liu, R., Song, F., Shen, X., 2014. Magnetic nanocomposite Ba-ferrite/α-iron hollow microfiber: a multifunctional 1D space platform for dyes removal and microwave absorption. Ceram. Int. 40, 15585–15594. https://doi.org/10.1016/j.ceramint.2014.07.035.
Yirsaw, B.D., Megharaj, M., Chen, Z., Naidu, R., 2016. Environmental application and ecological significance of nano-zero valent iron. J. Environ. Sci. (China) 44, 88–98. https://doi.org/10.1016/j.jes.2015.07.016.
Yu, P., Yu, H., Sun, Q., Ma, B., 2019. Filter Paper Supported nZVI for Continuous Treatment of Simulated Dyeing Wastewater. pp. 1–8. https://doi.org/10.1038/s41598-019-47863-5.